Energetic Macroscopic Representation of a Hybrid Electric Locomotive and experimental characterization of Nickel-Cadmium battery cells

J. Baert*, S.Jemei*, D.Chamagne*, D.Hissel*, Senior Member IEEE, S.Hibon** and D.Hegy**.
* University of Franche-Comte, FEMTO-ST (Energy Department), UMR CNRS 6174, 90010 Belfort, France.
** Alstom Transport, 3 Avenue des Trois Chênes, 90000 Belfort, France.
E-Mail: jerome.baert@univ-fcomte.fr – samuel.hibon@transport.alstom.com

Acknowledgements

This work was supported by Alstom Transport Group, company developing the most complete range of systems, equipment and service in the railway market.

Keywords

“Hybrid Electric Vehicle (HEV)”, “Energy Storage”, “Rail vehicle”, “batteries”, “Ultra-Capacitors (UCs)”, “experimental characterization”.

Abstract

The series architecture of a Hybrid Electric Locomotive (HEL) using the Energetic Macroscopic Representation (EMR) is suggested in this paper. Indeed, the EMR organizes systems as interconnected sub-systems, improving modularity and flexibility. Firstly, primary and secondary sources’ dynamical models are developed using the EMR. Batteries, Ultra-Capacitors (UCs), rheostat, diesel driven generator set and the HEV load are concerned in this kind of application. Secondly, Nickel-Cadmium battery cells’ experimental characterization is presented. The structure of the used test bench, the developed protocol and the experimental results are discussed.

Introduction

The transport sector, which is causing increased congestion and pollution, needs to undergo transformation. Hybrid Electric Locomotives (HEL)s combine the environmental benefits of a catenary-electric locomotive with the higher overall energy efficiency and lower infrastructure costs of a diesel-electric. The FEMTO-ST and Alstom Transport partnership aims at studying an Internal Combustion Engine (ICE)-battery/ultra-capacitor hybrid switcher locomotive for the disintegration, organization, pull-out and changing railway lanes activities. Indeed, switcher locomotives are used in rail yards for assembling and disassembling trains and moving them from one point to another. Indeed, the figure 1 shows the evolution of the diesel driven generator set use for a typical shunting activity. Knowing that the ICE energy efficiency and pollution are very bad at lower loads but are improved at higher loads, the current configuration is not optimal. The technology for hybridization is now available and has already been applied to other switcher locomotives, which are subject mainly to the shunting activities where brake energy recovery is most effective. The Chinese Dongfeng 7G HEL [1], the Iranian G12 HEL [2], the American Railpower Green Goat [3, 4] and the French Plathee project [5], recommend the use of the hybrid technology to regenerate energy from braking and store it effectively with batteries and/or ultra-capacitors. These studies underline the challenges related to issues of system layout, to the fuel consumption reduction, to a better maneuver, to the maintenance cost saving.

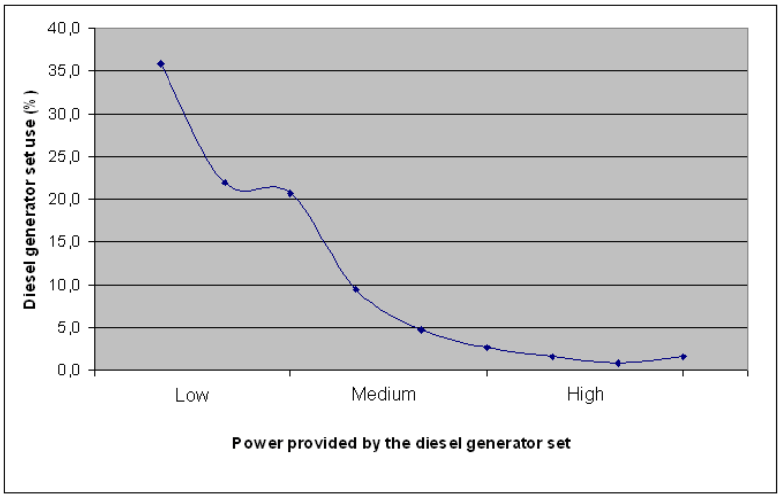

Fig. 1: Diesel driven generator set use according to the delivered power

The first study available in [6] presents the sizing of the secondary sources of the HEL. In the case of a multi-physical system graphical descriptions (bond graphs [7], power oriented graphs [8], or causal ordering graphs [9]) are well suited for the modeling. The Energetic Macroscopic Representation (EMR) is a synthetic representation for complex systems. The formalism aims at modeling interactions between systems and sub-systems. The representation is based on the integral causality and graphically shows the action and reaction phenomena between a system and its environment. The different used pictograms and colors permit a quick identification of the different elements of a system.

After implementing the dynamical models of the diesel driven generator set, the batteries and the ultra-capacitors and their local control structures, it is identified that the batteries modeling suffers from insufficiencies. In this paper, the dynamical models of the different on-board sources using the EMR are presented. Their respective Maximum and Practical Control Structures (M/PCSs) are also developed. Moreover, experimental characterizations' results are proposed to improve the insufficiencies of the batteries model. They mainly integrate their behavior according to the working temperature.

Architecture and modeling of the hybrid electric powertrain

In diesel-electric transmission systems, the mechanical energy produced by the diesel engine is converted into electricity. The conversion is performed thanks to generator and the electricity is transferred to an electric traction drive. This electricity supplies the traction drive and auxiliaries (lighting, heating...). In diesel-electric propulsions, the ICE is optimally used in a limited speed range. Diesel-electric locomotives do not need a catenary. Thus, the driver controls the power flow from the diesel driven generator set to the wheels by selecting the position of the throttle handle. The hybridization permits to deport a part of the power required by the activity on the other on-board sources. The selected architecture is a series one. All traction power is converted from electricity. A Direct Current (DC) bus ensures the electrical energy balance of the system. The primary source is not mechanically coupled to the powertrain but is coupled to an electrical generator to supply energy to the DC bus. The architecture presents some benefits for the engine use. It never idles and it can continuously operate in its most efficient region. The figure 2 presents the architecture of the HEL. The sources (ICE, batteries, ultra-capacitors), the rheostat, the traction motor, the auxiliaries and the local controls are represented. Moreover, the Energy Management Strategy (EMS) is also depicted but is not tackled in this paper.

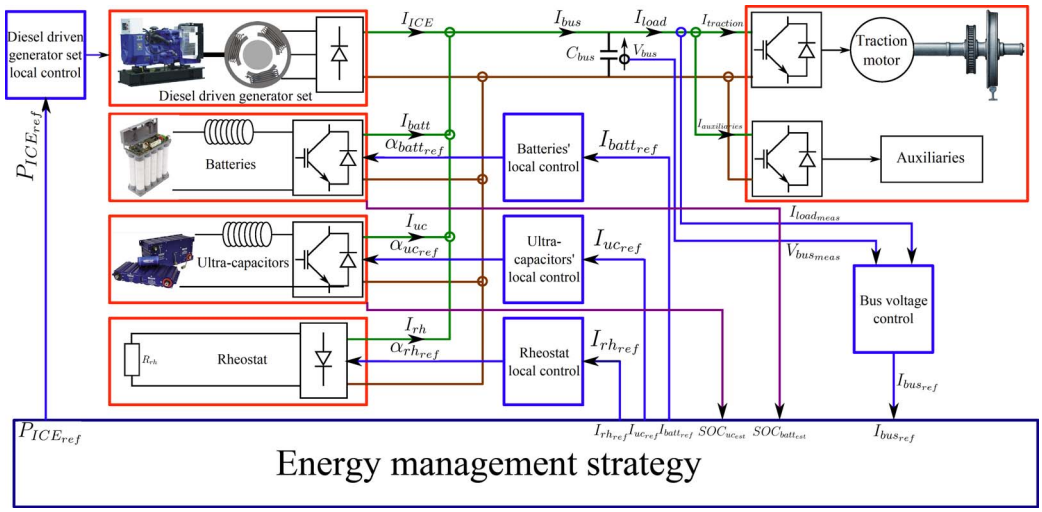

Fig. 2: Global architecture of the system

Diesel driven generator set modelling

The design of diesel engine is mostly alike the one of the gasoline engine. Both of them have pistons, cylinders and valves. However the ignition system in diesel engines is different. Instead of using the usual spark ignition, the fuel-air mixture is ignited by high temperature of the compressed air in the diesel engines. The steps of the process are the induction stroke, the compression stroke, the compression ignition, the power stroke, the exhaust stroke and the exhaust and inlet valve overlap.

The naturally aspirated diesel engine proposed in [10] is the adopted structure. The model takes into account the modeling of the ambient air which is characterized by a volume flow rate ($\dot{m}_{air}$) and a pressure (P_{air}), the intake manifold (equation 1), the throttle valve which is taken into account in the MCS, the cylinders (equation 2), the mechanical crank shaft (equation 3) and the fuel tank characterized by the exergy rate of the fuel (E_{xfuel}) and its mass flow rate ($\dot{m}_{fuel}$).

$$\frac{dP_{im}(t)}{dt} = \frac{RT_{im}}{V_{im}}\left(\dot{m}_{air}(t) - \dot{m}_{cyl}(t)\right) \tag{1}$$

where R is the ideal gas constant, $\dot{m}_{air}(t)$ and $\dot{m}_{cyl}(t)$ represent the in and out mass flows, T_{im} is the temperature of the air and P_{im} its pressure.

$$\begin{cases} T_{cyl} = \frac{1}{\Omega_{shaft}}\left(\eta_{ind}\dot{m}_{fuel}E_{x_{fuel}} - \frac{\Omega_{shaft}}{4\pi}V_{ed}(P_{air} - P_{im})\right) \\ \dot{m}_{cyl} = \frac{P_{im}}{RT_{im}}\eta_v\frac{\Omega_{shaft}}{4\pi}V_{ed} \end{cases} \tag{2}$$

with V_{ed} the displacement of the engine, η_{ind} the global (fuel - torque) efficiency, η_v the volumetric efficiency, T_{cyl} the produced torque and Ω_{shaft} the rotational speed of the shaft.

$$J\frac{d\Omega_{shaft}(t)}{dt} = T_{cyl}(t) - T_{load}(t) - f_{shaft}\Omega_{shaft}(t) \tag{3}$$

with J the inertia of the shaft and f_{shaft} the damping forces. The built MCS permits to control the shaft rotational speed.

To convert the mechanical power produced by the diesel engine into an electrical power and to deliver it to the central DC bus, an alternator (salient pole synchronous machine) is coupled to the ICE. The modeling is based on the work of [11] and [12]. The PCS permits to control the mechanical load torque. Coupled with the diesel engine EMR and MCS (figure 3), the mechanical power at the output of the shaft is controlled.

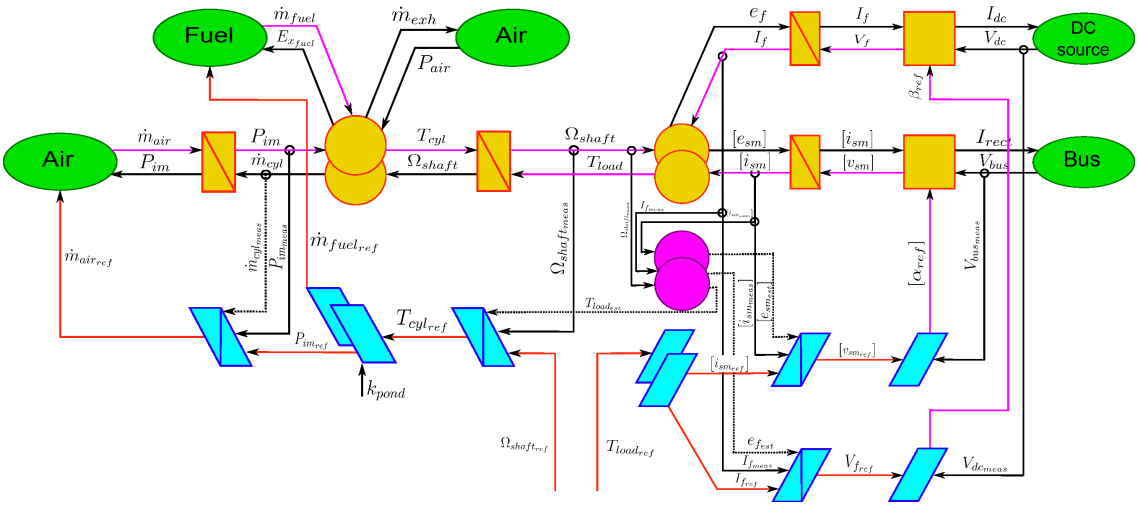

Fig. 3: Modelling of the diesel driven generator set

Ultra-Capacitors modelling

An ultra-capacitor shares several of the basic characteristics of a normal capacitor. The electrodes are typically constructed by applying a layer of activated carbon to a layer of metal foil. The electrodes are submersed in an electrolytic fluid, and separated by a thin separator which acts as an electronic insulator between the electrodes and a conduit for ion transport. They are used in numerous applications in order to provide peak power requirement. The principal advantage of the ultra-capacitor compared to the battery, is that it can support several tens of thousands of cycles of charge/discharge with very high currents.

The adopted ultra-capacitor's cell model is based on an equivalent circuit consisting in two RC branches is used (figure 4 – equation 4 – [13]). The first or immediate branch, with the elements Ri, Ci0 and the voltage-dependent capacitor Ci1 (in F/V), dominates the immediate behavior of the capacitor in the time range of seconds in response to a charge action. The second or delayed branch, with parameters Rd and Cd dominates the terminal behavior in the range of minutes. Ri - Rd are resistances and Ci1×Vci - Ci0 - Cd are capacitance.

$$\begin{cases} i_1(s) = i(s) - \dfrac{V_t(s)}{R_d + \frac{1}{C_d s}} \\ V_t(s) = R_i i_1(s) + \dfrac{i_1(s)}{(C_{i0} + C_{i1} V_t(s))s} \end{cases} \quad (4)$$

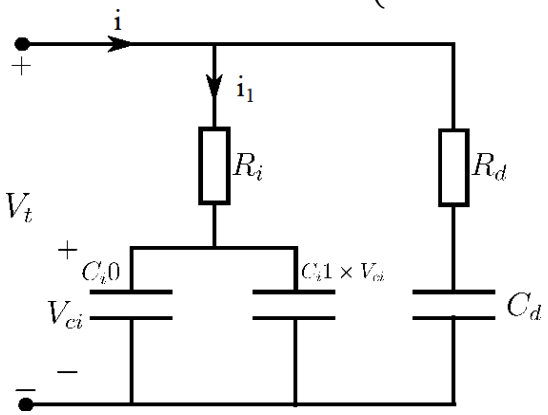

Fig. 4: Equivalent circuit model for an ultra-capacitor's cell.

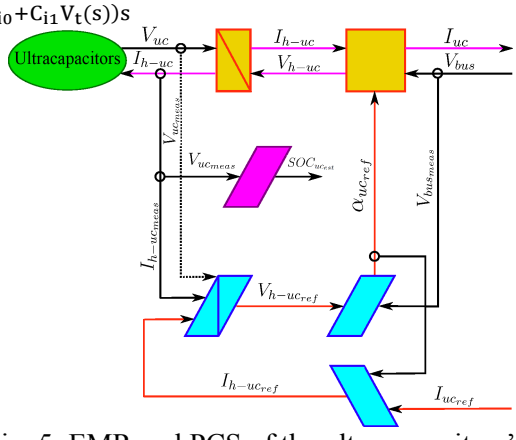

Fig. 5: EMR and PCS of the ultra-capacitors' pack

The corresponding EMR and M/PCS of the ultra-capacitors' part are depicted on figure 5. The used estimation block estimates the State Of Charge (SOC) of the elements linked to their power electronics

(filter and chopper). The power electronics aim at performing the adequacy of power between the source and the rest of the system thanks to the central DC bus.

Batteries modelling

The NiCd battery is a type of rechargeable battery using nickel oxide hydroxide and metallic cadmium as electrodes [14]. Compared to other batteries' technology (Lithium-Ion, Lead-Acid, Carbon-Zinc), they tolerate deep discharge for long period, they last longer in terms of number of charge/discharge cycles, their terminal voltage declines slower when discharging, their capacity is not significantly affected by very high discharge currents. Compared to NiCd batteries, NiMH batteries have a higher capacity and are less toxic, and are now more cost effective. However, a NiCd battery has a lower self-discharge rate (20% per month for a NiCd battery versus 30% per month for a traditional NiMH under identical conditions).

Based on [15], [16], an improved and easy-to-use battery cell dynamic model is presented. The discharge model is similar to the Shepherd model and accurately represents the voltage dynamics when the current varies and takes into account the Open Circuit Voltage (OCV) as a function of the SOC. A term concerning the polarization voltage is added to better represent the OCV behavior. The equation 5 gives the battery discharge model.

$$V_{batt} = E_0 - Ri - K_1 \frac{Q}{Q-it} i^* - K_2 \frac{Q}{Q-it} it + Ae^{-B.it} \quad (5)$$

with V_{batt} the battery voltage, E_0 the battery constant voltage, K_2 the polarization constant, K_1 the polarization resistance, Q the battery capacity, it the actual battery charge, R the internal resistance, i the battery applied current, i* the filtered current, A the exponential zone amplitude and B the exponential zone time constant inverse.

The charge model is represented equation 6.

$$V_{batt} = E_0 - Ri - K_1 \frac{Q}{|it|-0.1Q} i^* - K_2 \frac{Q}{|it|-0.1Q} it + Ae^{-B.it} \quad (6)$$

The filtered current is used to flow through the polarization resistance which term models the nonlinear variations of the OCV with the SOC. The used technology presents a hysteresis phenomenon between the charge and the discharge phases which only occurs in the exponential area. The hysteresis phenomenon is taken into account in the exponential term of the equations. In theory, when it = 0 (fully charged), the polarization resistance is infinite. In practice, the contribution of the polarization resistance is shifted by about 10% of the capacity of the battery. The corresponding EMR and M/PCS of the batteries' part are depicted on figure 6. The used estimation block also estimates the State Of Charge (SOC) of the elements linked to their power electronics (filter and chopper).

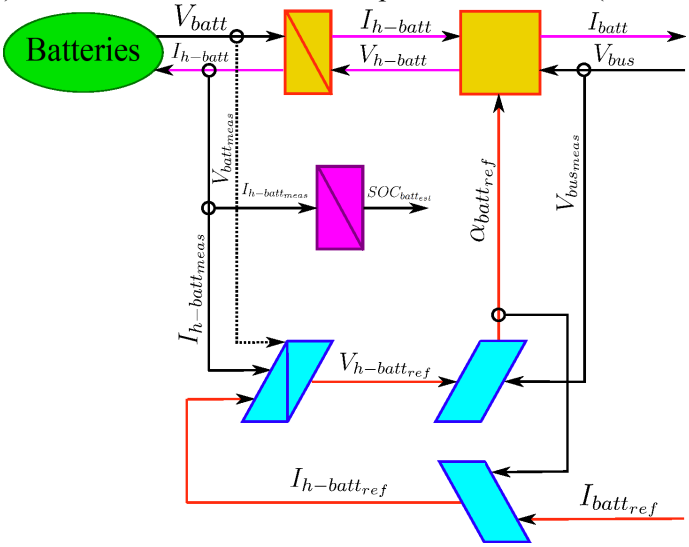

Fig. 6: EMR and PCS of the batteries' pack

Experimental characterization of the batteries

The drawback of the batteries' model remains to use a constant internal resistance value (R) of the cell. However, the internal resistance mainly depends on the cell's SOC and the working temperature. Thus, to establish this dependency, an experimental test bench is developed (figure 7 and figure 8 - [17]). The test bench is made up of a control unit to record data and to apply current's references, a thermal chamber to perform temperature tests and power electronics (power source and electronic load) to charge or discharge the cell. The protocol consists in fully charging/discharging the element with some current rates and recording data such as:

- the anode, cathode, surface and room temperatures,
- the source, load and cell currents,
- the source, load and cell voltages.

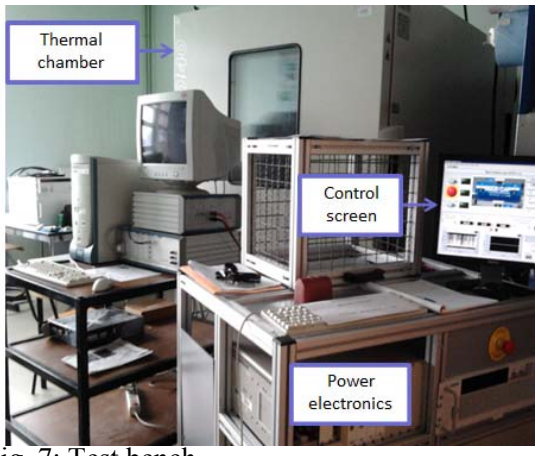

Fig. 7: Test bench

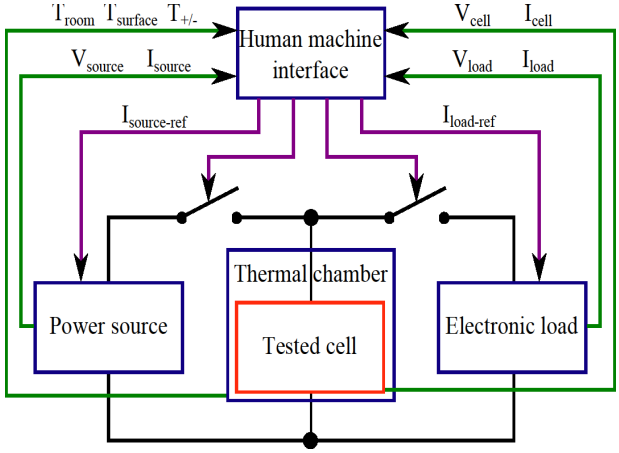

Fig. 8: Test bench structure

Contactors are also set up to provide the electrical separation of the charge and discharge circuits. Till today, the performed tests stand for C5 and C3 rates and for six working temperatures (-50°C, -40°C, -20°C, 0°C, 20°C and 40°C). A Cx rate corresponds to a current which permits to charge/discharge the element during x hours. Thus, in theory a C5 (respectively C3) rate permits to charge/discharge the element in 5 (respectively 3) hours. The internal resistance (R) is calculated each 10% of the cell's SOC (equation 7).

$$R = \frac{\Delta V}{\Delta I} \tag{7}$$

with ΔV the voltage variation and ΔI the current one (C5 and C3 rates).

The figure 9 (respectively figure 10) presents the evolution of the calculated internal resistance value of a single cell according to its SOC and the working temperature for a C5 current rate (respectively C3).

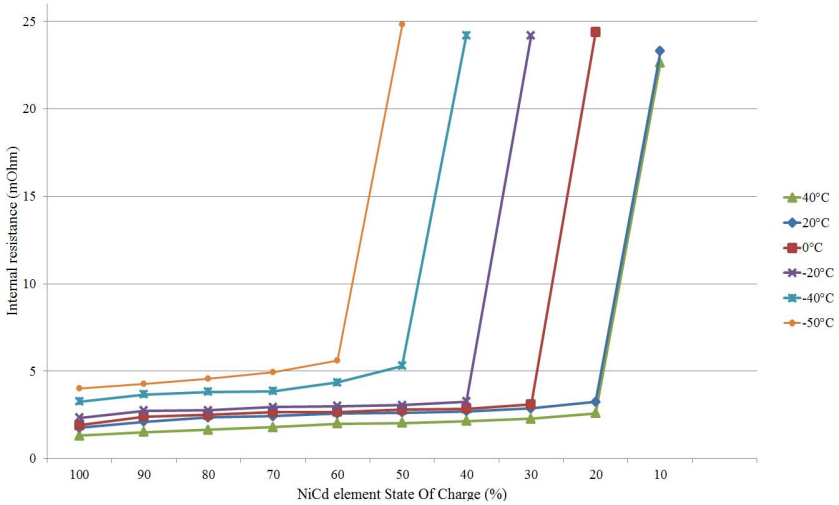

Fig. 9: Internal resistance of a cell according to the SOC and temperatures (C5 current rate)

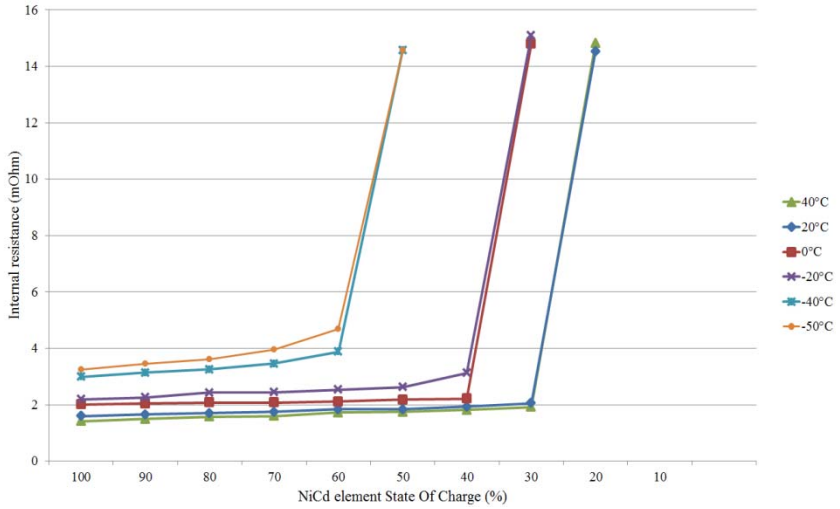

Fig. 10: Internal resistance of a cell according to the SOC and temperatures (C3 current rate)

The figure 9 and the figure 10 clearly show that the internal resistance value depends on its SOC and the temperature. It increases with the SOC and with the lowest temperatures (negative ones). Considering the positive temperatures (20°C and 40°C), its value does not vary a lot. However, for negative temperatures (especially -50°C and -40°C), this value is higher and it is impossible to fully discharge the cell. Indeed, only the half of the capacity is available at -50°C which is due to the partial freezing of the electrolyte. Experiments have shown that this electrolyte is available again when the cell is warmed up. Moreover, the two figures emphasize the ageing effect of the cell. For instance, at -40°C, 0°C, 20°C and 40°C, the cell is fully discharged for the first experiment (C5 – figure 9) when reaching 40%, 20% and 10% for the SOC whereas at the same temperatures during the second experiment (C3 - figure 10), the cell is fully discharged when reaching 50%, 30% and 20%.

The next results from the figure 11 to the figure 18 confirm the obtained results. They represent the real evolution of the voltage of a single cell according to time for a full discharge and the response of the Simulink model which integrates the internal resistance variation now.

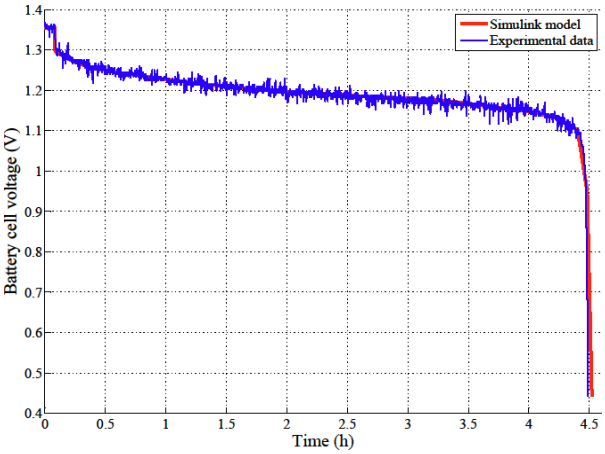

Fig. 11: NiCd's cell model validation for 40°C (C5)

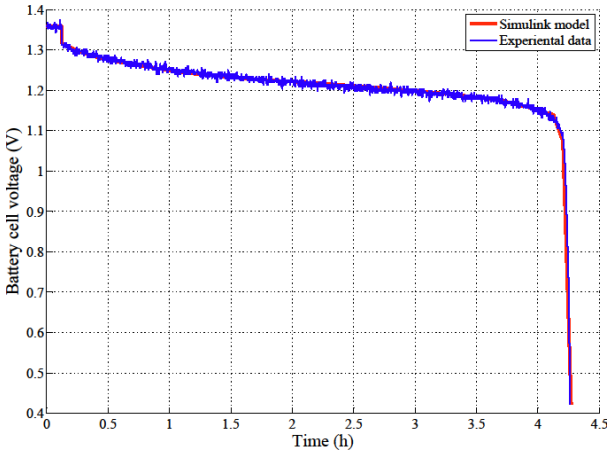

Fig. 12: NiCd's cell model validation for 20°C (C5)

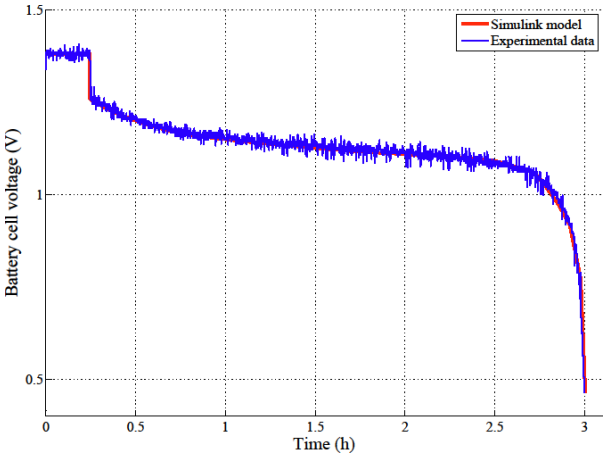

Fig. 13: NiCd's cell model validation for -40°C (C5)

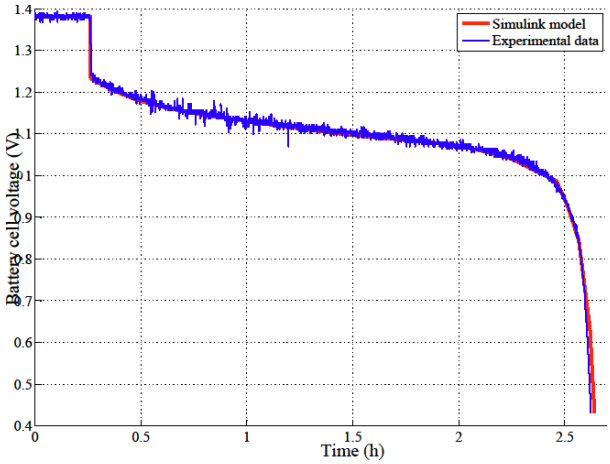

Fig. 14: NiCd's cell model validation for -50°C (C5)

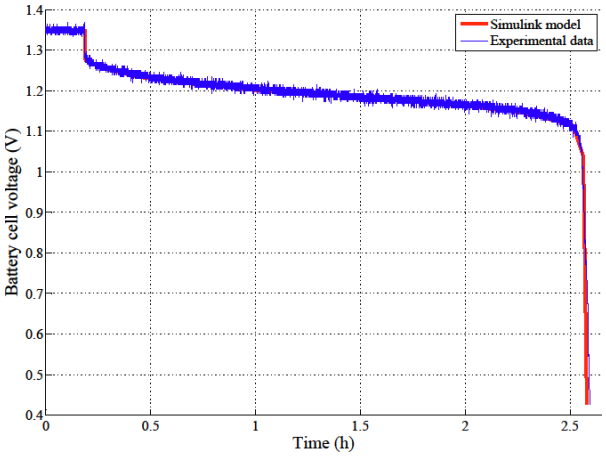

Fig. 15: NiCd's cell model validation for 40°C (C3)

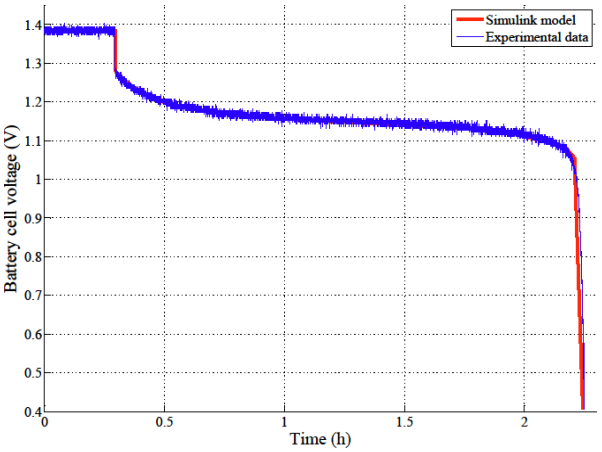

Fig. 16: NiCd's cell model validation for 20°C (C3)

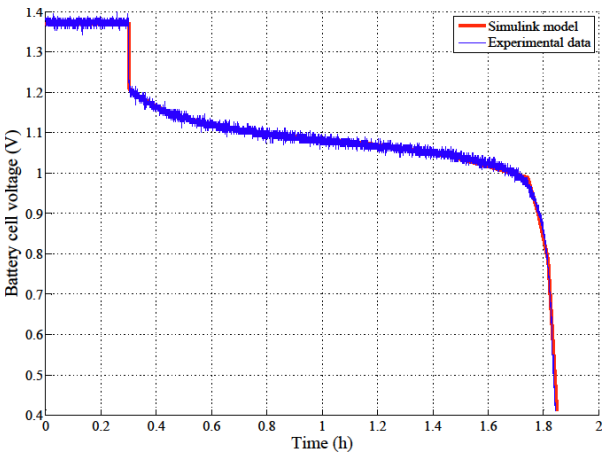

Fig. 17: NiCd's cell model validation for -40°C (C3)

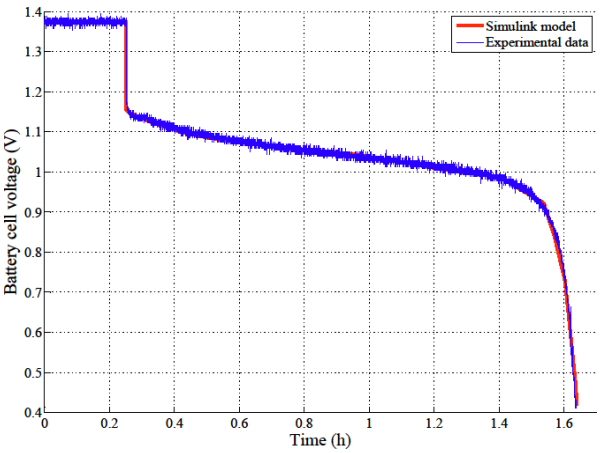

Fig. 18: NiCd's cell model validation for -50°C (C3)

Instead of discharging the element in around 4.25h at room temperature (C5 - figure 12) or in 2.6h (C3 - figure 16), the discharge only takes 2.6h at -50°C (C5 – figure 14) or 1.6h (C3 – figure 18). Indeed, a part of the electrolyte is unavailable due to the partial freezing of the electrolyte. Indeed, the electrolyte concentration does not change with the SOC. Thus, even a fully discharged battery is no more susceptible to freezing than one that is charged. Also, rather than freezing solid, the electrolyte tends to become slushy at extremely low temperatures and the battery is still able to function. Provided

 ISBN: 978-90-75815-17-7 and 978-1-4799-0114-2

that the capacity is adequately compensated for low operating temperatures, no further consideration for cold weather is required.

EMR of the series hybrid electric powertrain

Figure 19 presents the selected architecture of the hybrid electric locomotive using EMR. Primary source (diesel driven generator set), secondary sources (batteries, ultra-capacitors), the rheostat and the load (power mission of the locomotive) are linked to a central DC bus thanks to the on-board power electronics. The model is made up of the previous presented dynamical models of the sources. The EMS which is not the goal of the paper is represented by the strategy block. It aims at defining the powers' references to be delivered/recovered by the on-board sources in order to ensure the considered driving cycle. The EMS must take into account the sources characteristics (SOC, reversibility…), the system state (speed, power requirements…) and ensure the bus voltage stability. The EMS study is detailed in [18].

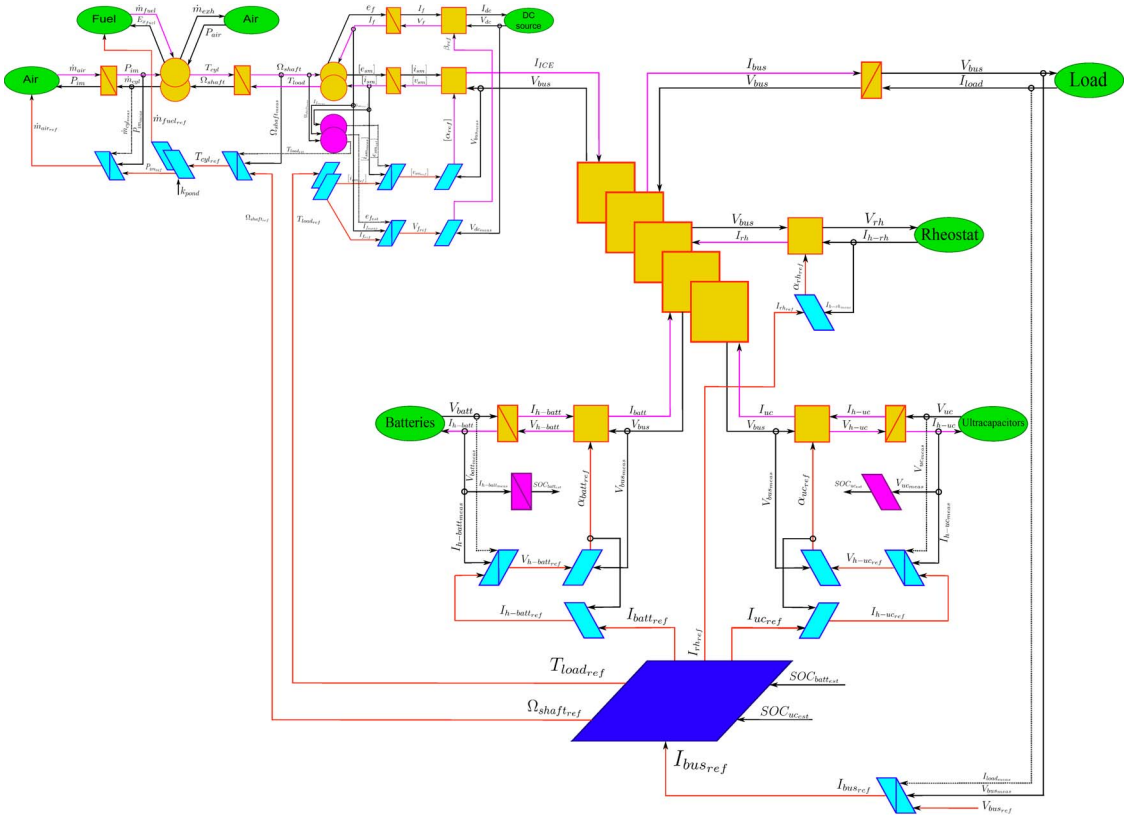

Fig. 19: EMR architecture of the system

Conclusion

An overall Hybrid Electric Locomotive Energetic Macroscopic Representation has been developed. The new proposed EMR/PCS of the internal combustion engine is a dynamical model and informs about the injected fuel type. It respects the principles of physical causality and interaction and permits to identify the interconnected elements (intake manifold, throttle valve, cylinders…). The batteries and ultra-capacitors' models are also dynamical models. Their PCS emphasizes the SOC estimation of the elements. Moreover, the internal resistance behavior of the battery's cell model has been improved thanks to experimental characterizations on a test bench. They aim at simulating as well as possible the real behavior of a NiCd cell. The NiCd cells internal resistance evolution greatly depends on the working temperature and also to a lesser extent on the SOC. Further studies will focus on the ageing effect of the batteries. These first experiments show the importance of this phenomenon. Moreover, it influences the efficiency of the developed HEL, its maintenance cost and the EMS' specifications to limit the ageing.

ISBN: 978-90-75815-17-7 and 978-1-4799-0114-2

References

[1] Z. Xin and T. Yi, “Research of hybrid electric locomotive control strategy”. In: 2011 International Conference on System Science, Engineering Design and Manufacturing Informatization (ICSEM), pp. 118-122, 2011.

[2] B. Asaei and M. Amiri, “High Efficient Intelligent Motor Control for a Hybrid Shunting Locomotive”, In: Vehicle Power and Propulsion Conference, 2007. VPPC 2007. IEEE, pp. 405-411, 2007.

[3] R. Cousineau, “Development of a hybrid switcher locomotive the Railpower Green Goat”, Instrumentation Measurement Magazine, IEEE, Vol. 9, No. 1, pp. 25-29, 2006.

[4] A. Miller, K. Hess, D. Barnes, and T. Erickson, “System design of a large fuel cell hybrid locomotive”, Journal of Power Sources, Vol. 173, No. 2, pp. 935-942, 2007. X Polish Conference on Systems with Fast Ionic Transport.

[5] C. Akli, X. Roboam, B. Sareni, and A. Jeunesse, “Energy management and sizing of a hybrid locomotive”, 2007 European Conference on Power Electronics and Applications, pp. 1 –10, 2007.

[6] J. Baert, S. Jemei, D. Chamagne, D. Hissel, S. Hibon, and D. Hegy, “Sizing of a hybrid locomotive,” IEEE Vehicle Power and Propulsion Conference, 2011, VPPC ’11, pp. 1 – 6, 2011.

[7] T. Bakka and H.R. Karimi, "Wind turbine modeling using the bond graph," IEEE International Symposium on Computer-Aided Control System Design (CACSD), 2011, pp.1208-1213, 28-30 Sept. 2011.

[8] R. Zanasi and F. Grossi, "Differences and common aspects of POG and EMR energy-based graphical techniques," Vehicle Power and Propulsion Conference (VPPC), 2011 IEEE, pp.1-6, 6-9 Sept. 2011.

[9] Bouscayrol, R. Schoenfeld, G. Dauphin-Tanguy, G.-H. Geitner, X. Guillaud, A. Pennamen and J.P. Hautier, "Different energetic descriptions for electromechanical systems," European Conference on Power Electronics and Applications, 2005, pp.1-10.

[10] Verdonck, N., Chasse, A., Pognant-Gros, P. and Sciarretta, A. (2010). Automated Model Generation for Hybrid Vehicles Optimization and Control. Oil Gas Sci. Technol. Rev. IFP, Vol. 65, No. 1, pp. 115-132.

[11] J. Heywood, Internal combustion engine fundamentals, ser. McGraw-Hill series in mechanical engineering. McGraw-Hill, 1988. Available: http://books.google.fr/books?id=O69nQgAACAAJ

[12] Bouscayrol, A., Delarue, P. and Guillaud. X. (2005). Power strategies for maximum control structure of a wind energy conversion system with a synchronous machine. Renewable Energy, Vol. 30, No. 15, pp. 2273-2288.

[13] L. Zubieta and R. Bonert, “Characterization of double-layer capacitors for power electronics applications,” IEEE Transactions on Industry Applications, vol. 36, no. 1, pp. 199 –205, jan/feb 2000.

[14] Boulon, L.; Hissel, D.; Bouscayrol, A.; Pera, M.C.; Delarue, P.; , "Multi physics modelling and representation of power and energy sources for Hybrid Electric Vehicles," Vehicle Power and Propulsion Conference, 2008. VPPC '08. IEEE, vol., no., pp.1-6, 3-5 Sept. 2008

[15] O. Tremblay, L.-A. Dessaint, and A.-I. Dekkiche, “A generic battery model for the dynamic simulation of hybrid electric vehicles,” in Vehicle Power and Propulsion Conference, 2007. VPPC 2007. IEEE, sept. 2007, pp. 284 –289.

[16] O. Tremblay, “Experimental validation of a battery dynamic model for ev applications,” World Electric Vehicle Journal, vol. 3, 2009.

[17] N. Devillers, S. Jemei, M.C. Péra, D. Bienaimé, F. Gustin, “Characterization for Lithium-ion polymer Secondary Battery Modelling”, Journal of Power Sources, on submission.

[18] J. Baert, S. Jemei, D. Chamagne, D. Hissel, S. Hibon, D. Hegy, "Intelligent Energy Management Strategy of a Hybrid Electric Locomotive based on optimized Type-1 and Type-2 Fuzzy Logic Controllers", IEEE Transactions on Industrial Informatics, on reviewing.